Plasmon resonant coupling in metallic nanowires

Jörg P. Kottmann and Olivier J.F. Martin

Electromagnetic Fields and Microwave Electronics Laboratory
Swiss Federal Institute of Technology, ETH–Zentrum, 8092 Zurich, Switzerland

kottmann@ifh.ee.ethz.ch,martin@ifh.ee.ethz.ch
http://www.ifh.ee.ethz.ch/~martin

Abstract: We investigate the plasmon resonances of interacting silver nanowires with a 50 nm diameter. Both non–touching and intersecting configurations are investigated. While individual cylinders exhibit a single plasmon resonance, we observe much more complex spectra of resonances for interacting structures. The number and magnitude of the different resonances depend on the illumination direction and on the distance between the particles. For very small separations, we observe a dramatic field enhancement between the particles, where the electric field amplitude reaches a hundredfold of the illumination. A similar enhancement is observed in the grooves created in slightly intersecting particles. The topology of these different resonances is related to the induced polarization charges. The implication of these results to surface enhanced Raman scattering (SERS) are discussed.

OCIS codes: (160.3900) Metals; (240.5420) Polaritons; (260.3910) Metals, optics of; (290.0290) Scattering; (260.5740) Resonance; (290.5860) Raman scattering; (350.3950) Micro-optics; (350.4990) Particles.

References and links

1. K. Bromann, C. Félix, H. Brune, W. Harbich, R. Monot, J. Buttet, and K. Kern, "Controlled Deposition of Size-Selected Silver Nanoclusters," Science **274,** 956–958 (1996).
2. K. Abe, T. Hanada, Y. Yoshida, N. Tanigaki, H. Takiguchi, H. Nagasawa, M. Nakamoto, T. Yamaguchi, and K. Yase, "Two-dimensional array of silver nanoparticles," Thin Solid Films **327-329,** 524–527 (1997).
3. J. C. Hulteen, D. A. Treichel, M. T. Smith, M. L. Duval, T. R. Jensen, and R. P. van Duyne, "Nanosphere Lithography: Size-Tunable Silver Nanoparticles and Surface Cluster Arrays," J. Phys. Chem. B **103,** 3854–3863 (1999).
4. D. Y. Petrovykh, F. J. Himpsel, and T. Jung, "Width distribution of nanowires grown by step decoration," Surf. Science **407,** 189–199 (1998).
5. G. L. Che, B. B. Lakshmi, E. R. Fisher, and C. R. Martin, "Carbon nanotubule membranes for electrochemical energy storage and production," Nature **393,** 346–349 (1998).
6. A. P. Li, F. Müller, and U. Gösele, "Polycrystalline and Monocrystalline Pore Arrays with Large Interpore Distance in Anodic Alumina," Electrochem. Solid-State Lett. **3,** 131–134 (2000).
7. R. Elghanian, J. J. Storhoff, R. C. Mucic, R. L. Letsinger, and C. A. Mirkin, "Selective Colorimetric Detection of Polynucleotides Based on the Distance-Dependent Optical Properties of Gold Nanoparticles," Science **277,** 1078–1081 (1997).
8. L. A. Lyon, M. D. Musick, and M. J. Natan, "Colloidal Au-Enhanced Surface Plasmon Resonance Immunosensing," Anal. Chem. **70,** 5177–5183 (1998).
9. S. Schultz, D. R. Smith, J. J. Mock, and D. A. Schultz, "Single-target molecule detection with nonbleaching multicolor optical immunolabels," Proc. Natl. Acad. Sci. USA **97,** 996–1001 (2000).
10. C. Viets and W. Hill, "Single-fibre surface-enhanced Raman sensors with angled tips," J. Raman Spectrosc. **31,** 625–631 (2000).
11. T. J. Silva and S. Schultz, "A scanning near-field optical microscope for the imaging of magnetic domains in reflection," Rev. Sci. Inst. **67,** 715–725 (1996).

#33954 - $15.00 US
Received May 09, 2001; Revised May 25, 2001

12. R. M. Stöckle, Y. D. Suh, V. Deckert, and R. Zenobi, "Nanoscale chemical analysis by tip-enhanced Raman spectroscopy," Chem. Phys. Lett. **318,** 131–136 (2000).
13. J. P. Kottmann and O. J. F, "Retardation-induced plasmon resonances in coupled nanoparticles," Opt. Lett. **in press** (2001).
14. M. Quinten, A. Leitner, J. R. Krenn, and F. R. Aussenegg, "Electromagnetic energy transport via linear chains of silver nanoparticles," Opt. Lett. **23,** 1331–1333 (1998).
15. J.-C. Weeber, A. Dereux, C. Girard, J. R. Krenn, and J.-P. Goudonnet, "Plasmon polaritons of metallic nanowires for controlling submicron propagation of light," Phys. Rev. B **60,** 9061–9068 (1999).
16. J. R. Krenn *et al.*, "Squeezing the optical near–field by plasmon coupling of metallic nanoparticles," Phys. Rev. Lett. **82,** 2590–2593 (1999).
17. J. Tominaga, C. Mihalcea, D. Büchel, H. Fukuda, T. Nakano, N. Atoda, H. Fuji, and T. Kikukawa, "Local plasmon photonic transistor," Appl. Phys. Lett. **78,** 2417–2419 (2001).
18. M. Moskovits, "Surface-enhanced spectroscopy," Rev. Mod. Phys. **57,** 783–826 (1985).
19. K. Kneipp, Y. Wang, H. Kneipp, L. T. Perelman, I. Itzkan, R. R. Dasari, and M. S. Feld, "Single molecule detection using surface-enhanced Raman scattering," Phys. Rev. Lett. **78,** 1667–1670 (1997).
20. S. Nie and S. R. Emory, "Probing single molecules and single nanoparticles by surface-enhanced Ramsn scattering," Science **275,** 1102–1106 (1997).
21. H. Xu, E. J. Bjerneld, M. Käll, and L. Börjesson, "Spectroscopy of Single Hemoglobin Molecules by Surface Enhanced Raman Scattering," Phys. Rev. Lett. **83,** 4357–4360 (1999).
22. J. P. Kottmann, O. J. F. Martin, D. R. Smith, and S. Schultz, "Dramatic localized electromagnetic enhancement in plasmon resonant nanowires," Chem. Phys. Lett. **in press,** (2001).
23. J. P. Kottmann, O. J. F. Martin, D. R. Smith, and S. Schultz, "Spectral response of Silver nanoparticles," Optics Express **6,** 213–219 (2000).
24. J. P. Kottmann, O. J. F. Martin, D. R. Smith, and S. Schultz, "Plasmon resonances of silver nanowires with a non–regular cross–section," Phys. Rev. B submitted (2001).
25. F. J. García-Vidal and J. B. Pendry, "Collective theory for surface enhanced Raman scattering," Phys. Rev. Lett. **77,** 1163–1166 (1996).
26. P. K. Aravind, A. Nitzan, and H. Metiu, "The interaction between electromagnetic resonances and its role in spectroscopic studies of molecules adsorbed on colloidal particles or metal spheres," Surf. Sci. **110,** 189–204 (1981).
27. A. I. Vanin, "Surface-amplified Raman scattering of light by molecules adsorbed on groups of spherical particles," J. Appl. Spectrosc. 62 (1995).
28. N. Félidj, J. Aubard, and G. Lévi, "Discrete dipole approximation for ultraviolet-visible extinction spectra simulation of silver and gold colloids," J. Chem. Phys. **111,** 1195–1208 (1999).
29. H. Xu, J. Aizpurua, M. Käll, and P. Apell, "Electromagnetic contributions to single-molecule sensitivity in surface-enhanced Raman scattering," Phys. Rev. E **62,** 1–7 (2000).
30. C. F. Bohren and D. R. Huffman, *Absorption and scattering of light by small particles* (Wiley, New York, 1983).
31. U. Kreibig and M. Vollmer, *Optical Poperties of Metal Clusters*, *Springer Series in Material Science Vol. 25* (Springer Verlag, Berlin, 1995).
32. U. Kreibig and C. v. Fragstein, "The Limitation of Electron Mean Free Path in Small Silver Particles," Z. Physik **224,** 307–323 (1969).
33. L. Genzel, T. P. Martin, and U. Kreibig, "Dielectric Function and Plasma Resonances of Small Metal Particles," Z. Physik B **21,** 339–346 (1975).
34. K.-P. Charlé, L. König, S. Nepijko, I. Rabin, and W. Schulze, "The Surface Plasmon Resonance in Free and Embedded Ag-Clusters in the Size Range 1,5 nm $< D <$ 30 nm," Cryst. Res. Technol. **33,** 1085–1096 (1998).
35. J.-Y. Bigot, V. Halté, J. C. Merle, and A. Daunois, "Electron dynamics in metallic nanoparticles," Chem. Phys. **251,** 181–203 (2000).
36. P. B. Johnson and R. W. Christy, "Optical constants of the noble metals," Phys. Rev. B **6,** 4370–4379 (1972).
37. J. P. Kottmann and O. J. F. Martin, "Accurate solution of the volume integral equation for high permittivity scatterers," IEEE Trans. Antennas Propag. **48,** 1719–1726 (2000).
38. J. P. Kottmann, O. J. F. Martin, D. R. Smith, and S. Schultz, "Field polarization and polarization charge distributions in plasmon resonant particles," New J. Phys. **2,** 27.1–27.9 (2000).
39. M. I. Stockmann, V. M. Shalaev, M. Moskovits, R. Botet, and T. F. George, "Enhanced Raman scattering by fractal clusters: Scale-invariant theory," Phys. Rev. B **46,** 2821–2830 (1992).

#33954 - $15.00 US Received May 09, 2001; Revised May 25, 2001

1. Introduction

Over the last twenty years, much interest has been devoted to metallic nano–structures, and in particular to the strong electromagnetic enhancement they can provide via the excitations of plasmon resonances. With the rapid advances in the fabrication of very small particles [1, 2, 3] and nanowires [4, 5, 6], their optical properties are now used in a wide range of applications, including biosensors [7, 8, 9, 10], near–field microscopy [11, 12, 13] and new optical devices [14, 15, 16, 17]. Since the plasmons are associated with large electromagnetic fields near the particle surface, they play a key role in surface enhanced Raman scattering (SERS) [18]. For specific configurations, this enhancement can be so large that it allows single molecule detection [19, 20, 21].

Recently we demonstrated that nanowires with a non–regular cross–section have a very complex spectrum of plasmon resonances: while a cylindrical particle exhibits one resonance and an elliptical particle two, we observed that five or more distinct resonances can be excited in a triangular nanoparticle [22]. A dramatic near–field enhancement, with amplitude several hundred times that of the illumination field was also observed at the vicinity of these non–regular particles [23]. This enhancement was orders of magnitudes larger than that observed on regular particles. For example, the field amplitude at the vicinity of a 20 nm triangular particle can exceed 400 times the illumination amplitude, while this enhancement is only 10 for a cylindrical particle with the same size [24]. Raman enhancement being proportional to the fourth power of the amplitude enhancement [18], our results indicate Raman enhancement in excess of 10^{12} for non–regular particles, while a cylindrical particle provides a mere 10^4 enhancement.

The objective of this paper is to demonstrate that cylindrical particles, although harmless individually, can also provide strong enhancement when they are coupled together. Infinite arrays of particles have been studied theoretically [25], while long chains of nanoparticles in the 200 nm range have been investigated experimentally [15, 16]. We shall concentrate here on a pair of interacting particles and illustrate the different coupling mechanisms that can occur. Some aspects of this coupling in spherical metal particles have been investigated by others [26, 27, 28, 29].

In Sec. 2 we briefly outline our model. Results are presented in Sec. 3 and we summarize in Sec. 4.

2. Model

The plasmon resonances of particles with dimensions down to 2 (nm) can be investigated using Maxwell's theory [30, 31]. Herein, the particles are described by their dispersion relation, i.e. by their complex permittivity $\varepsilon(\lambda) = \varepsilon'(\lambda) + i\varepsilon''(\lambda)$ as a function of the wavelength λ. For silver and gold this dispersion relation is quite complex in the optical range, as the plasma frequency ω_p of the conduction electron gas lies in this range. When the illumination frequency passes nearby ω_p, the real part $\varepsilon'(\lambda)$ of the dielectric function changes its sign, and for specific negative $\varepsilon'(\lambda)$ values, plasmon resonances can be excited in the structure. These specific values strongly dependent on the particle size and shape [24]. The width of the plasmon resonances, which is related to the scattering amplitude, depends on the imaginary part $\varepsilon''(\lambda)$ of the permittivity. This imaginary part, which accounts for damping, becomes a function of the particle size when its dimensions are similar to the bulk electron mean free path [31]. In that case, electron scattering at the particle boundary becomes a dominant effect, and the decrease of the electron mean free path leads to an increase of $\varepsilon''(\lambda)$ [32, 33, 31, 34, 35]. However, for particles in the 50 nm range, which are the focus the present study, the permittivity is nearly unaffected and we shall simply use the bulk experimental data obtained by Johnson and Christie [36].

#33954 - $15.00 US
Received May 09, 2001; Revised May 25, 2001

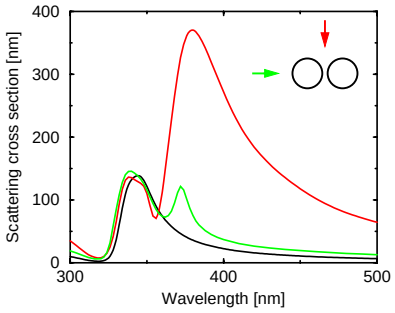

Fig. 1. SCS of two 50 nm diameter cylinders with a 5 nm separation. Two different illumination directions, indicated by the arrows in the inset, are considered. The SCS of a single cylinder is given for comparison (black).

Our numerical results are based on the finite elements method described in Ref. [37]. With this technique, we are able to accurately study the plasmon resonances of scatterers with an arbitrary shape [24]. Since we use a discretization in direct space, we can also investigate any arrangement of multiple scatterers, as is the case in the present work. Each cylinder section is discretized with about 1'500 triangular elements. A detailed convergence study of our numerical scheme is given in Ref. [37].

3. Results

Throughout the entire paper, we consider cylinders illuminated with a plane wave propagating in the plane of the figure, with the electric field in this plane as well (transverse electric polarization). All cylinders have a 50 nm diameter.

We first study two cylinders with a separation distance $d = 5$ nm. In Fig. 1 we show the scattering cross section (SCS) as a function of the wavelength λ for illumination along and normal to the major axis, the axis joining the cylinder centers (the illumination direction refers to the propagation direction of the illumination field; the incident electric field is therefore normal to this direction). The SCS of an individual 50 nm cylinder is also shown: in that case a single resonance is excited at $\lambda = 344$ nm. This resonance, although slightly blue shifted to $\lambda = 340$ nm, still exists in the coupled system for both illumination directions (Fig. 1). Note however that for the coupled system this resonance has the same magnitude as for the individual cylinder, although *two* cylinders are now scattering [especially for illumination from the top, where the incident field sees a broader structure, one would expect a larger SCS (Fig. 1)].

For illumination along the major axis we observe an additional resonance at $\lambda = 372$ nm. However, Fig. 1 clearly demonstrates that the coupling effect is much stronger

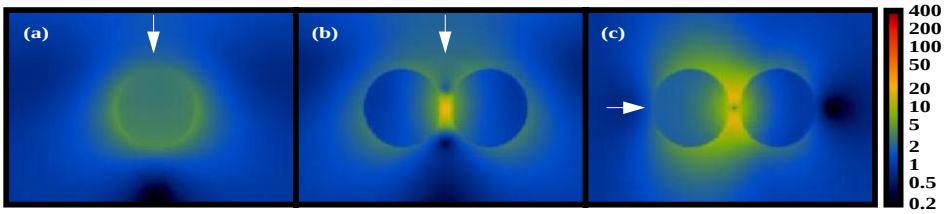

Fig. 2. Field amplitude distribution as a function of the illumination wavelength (indicated on the top of each frame) for (a) an individual cylinder (277 KB) and (b), (c) two interacting cylinders with a 5 nm separation (321 and 381 KB). The cylinders have 50 nm diameter. For the interacting cylinders two different illumination directions, indicated by the arrow, are considered. Front pictures: Corresponding main resonances (a) $\lambda = 344$ nm, (b)$\lambda = 380$ nm and (c) $\lambda = 374$ nm

.

#33954 - $15.00 US
Received May 09, 2001; Revised May 25, 2001

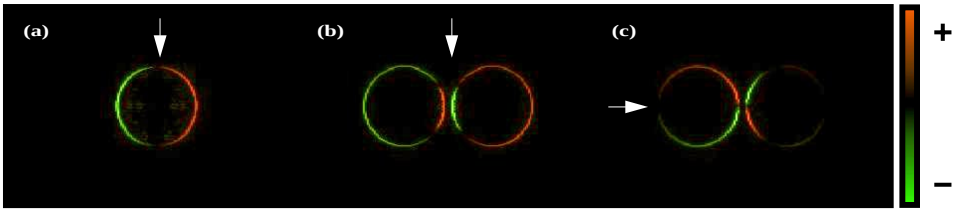

Fig. 3. Polarization charge distribution at the main resonance for (a) a single cylinder and (b), (c) two interacting cylinders with a separation $d = 5\,\mathrm{nm}$. Illumination direction as indicated. The cylinders have a 50 nm diameter. A different colorscale is used for each part: the charge density is much higher for the coupled cylinders (b) and (c) than for the single cylinder (a).

for incidence normal to the major axis (i.e. when the incident electric field is along the major axis). In that case we observe a rather broad resonance at $\lambda = 380\,\mathrm{nm}$ with a SCS amplitude much larger than that of the individual cylinder ($\lambda = 344\,\mathrm{nm}$).

The movies Figs. 2(a)–(c) show the electromagnetic near–field amplitude distribution corresponding to Fig. 1, as a function of the wavelength. For the single cylinder, the field distribution is very homogeneous, the field amplitude reaching about 8 (in units of the illumination amplitude) at the resonance ($\lambda = 344\,\mathrm{nm}$), and decreasing for larger wavelengths [Fig. 2(a)].

For the illumination normal to the major axis, the field amplitude in the interacting cylinders is homogeneous and rather weak, up to the single cylinder resonance wavelength [$\lambda = 344\,\mathrm{nm}$, Fig. 2(b)]. For larger wavelengths the coupling becomes quite strong, leading to a large field in the gap between the particles. There the field amplitude reaches almost 40 at the resonance ($\lambda = 380\,\mathrm{nm}$).

A similar enhancement is observed for the other illumination direction, with a field amplitude of 35 between the particles. The field distribution in the gap is however very different from the other illumination direction: The field now vanishes in the middle of the gap [Fig. 2(c)]. Retardation is essential for this resonance, as will be discussed later.

In Fig. 3 we show the polarization charge distribution associated with the main resonances reported in Fig. 2. This polarization charge distribution, which is given by the divergence of the electric field, oscillates in time: half a period later, the opposite charge distribution is observed [38]. The distributions in Fig. 3 correspond to a specific moment in time, when the magnitude of the instantaneous electric field vector is maximum in the gap. The moment when the near–field amplitude is maximum does not coincide with the moment when the illumination field is maximum, since – at resonance – there is a phase shift between the illumination and the particle response [38].

The polarization charge distribution in the single cylinder is symmetrical with respect to the illumination direction, with plus charges on one side of the particle and minus charges on the other side [Fig. 3(a)]. At the main resonance for the interacting cylinders illuminated from the top, polarization charge of opposite signs are confined on the sides of the gap [Fig. 3(b)]. Each particle remains of course neutral and a same amount of opposite charges is distributed on the remaining of the particle. Both cylinders are in phase, i.e. their charges distributions have negative charges on the left of the particle and positive charges on the right [Fig. 3(b)].

The polarization charge distribution at the main resonance for the other illumination direction is completely different [Fig. 3(c)]. In that case, both cylinders are out of phase, with respect to the illumination direction: the first (left) cylinder has $\pm$ charges, whereas the second (right) has $\mp$ charges [Fig. 3(c)]. This leads to a quadrupole–like charge distribution around the gap between the particles, which explains that the field vanishes in the middle of the gap, as observed in Fig. 2(c). This peculiar resonance can only be

#33954 - $15.00 US
Received May 09, 2001; Revised May 25, 2001

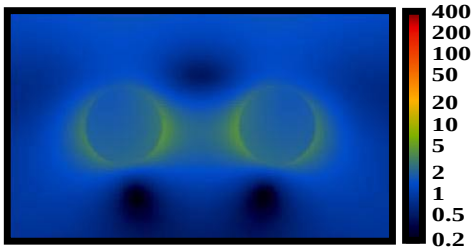

Fig. 4. Amplitude distribution for two interacting 50 nm cylinders for different separation distances d (negative distances correspond to intersecting cylinders) (283 KB). The corresponding main resonance wavelength is shown.

observed in particles large enough so that both cylinders are driven out of phase by the incident field. This coupling mechanism is therefore governed by retardation. It was investigated in Ref. [13], where we show that for silver cylinders, this coupled mode occurs only for particle diameters larger than 30 nm.

We now study the influence of the separation distance d on the plasmon resonant coupling. We shall focus on the illumination direction normal to the major axis as it provides the strongest coupling, particularly for small separation distances.

Figure 4 shows the field distribution for different separation distances d, at the corresponding main resonance wavelength (i.e. not at a constant wavelength). For a separation distance equal to the diameter, there is almost no coupling, whereas the field enhancement becomes very large for $d \leq 5$ nm. Around $d = 2$ nm the field amplitude in the gap exceeds 200 times that of the illumination field.

Negative separation distances in Fig. 4 correspond to intersecting cylinders. In that case we observe a large amplitude enhancement in the grooves, exceeding 100 times the illumination amplitude. Similar enhancement has also been obtained by García-Vidal *et al.* for an infinite array of cylinders embedded in a surface [25]. When the cylinders intersect further this enhancement decreases and the field distribution finally merges into that of the single cylinder (Fig. 4).

Let us emphasize that the over hundredfold enhancement of the illumination amplitude observed for small separations or intersections, corresponds to an intensity enhancement larger than 10^4. In SERS, where the Raman signal is in a good approximation proportional to the fourth power of the amplitude enhancement [18], this would lead to a local Raman enhancement in excess of 10^8.

We now study the spectral response for particular separation distances d. In Fig. 5 we report the SCS for $d = 2, 5, 10$ and 20 nm. The SCS clearly demonstrate that the main resonance is red–shifted with decreasing separation distance d, from 350 nm (d=50 nm) to 358 nm (d=20 nm), 368 nm (d=10 nm), 380 nm (d=5 nm) and 404 nm (d=2 nm).

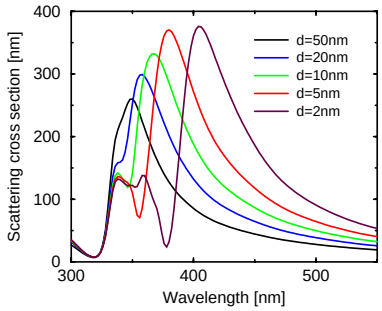

Fig. 5. SCS for two 50 nm cylinders illuminated normally to their main axis. Five separation distances are investigated: $d = 2, 5, 10, 20$ and 50 nm.

#33954 - $15.00 US
Received May 09, 2001; Revised May 25, 2001

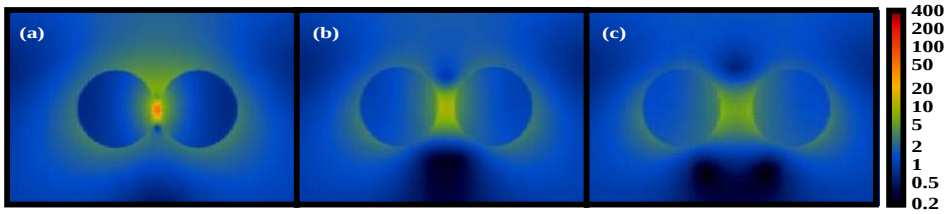

Fig. 6. Spectral variation of the field amplitude distribution for two interacting cylinders illuminated from the top, for different separation distances d: (a) $d = 2\,\mathrm{nm}$ (361 KB), (b) $d = 10\,\mathrm{nm}$ (359 KB), and (c) $d = 20\,\mathrm{nm}$ (313 KB). Front pictures: Corresponding main resonances (a) $\lambda = 404\,(\mathrm{nm})$, (b)$\lambda = 368\,(\mathrm{nm})$, and (c) $\lambda = 358\,(\mathrm{nm})$.

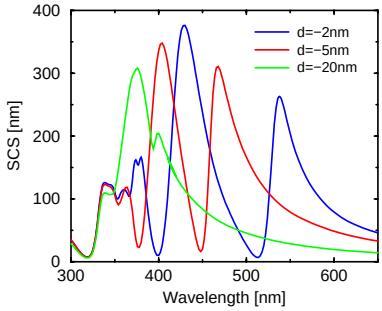

Fig. 7. SCS for two intersecting 50 nm cylinders illuminated from the top. Three intersection distances are investigated: $d = -2, -5$ and $-20\,\mathrm{nm}$.

Moreover, the complexity of the SCS increases for small separations, as higher order modes are excited (Fig. 5).

In Fig. 6 we report the spectral behavior of the field distributions for $d = 2, 10$ and $20\,\mathrm{nm}$ [the case d $= 5\,\mathrm{nm}$ is already shown in Fig. 2(b)]. The two higher order resonances at $\lambda = 350\,\mathrm{nm}$ and $\lambda = 362\,\mathrm{nm}$, visible in the SCS for $d = 2\,\mathrm{nm}$ (Fig. 5), are also visible in Fig. 6(a). Between 350 nm and 370 nm, we observe a rather complicated field distribution in the gap between the cylinders, related to the complex polarization charge distribution associated with these higher order modes [Fig. 6(a)]. These two resonances are closer than their width, and therefore strongly interfering, leading to the rapidly evolving field pattern visible at the vicinity of the gap. This pattern can be related to the charges distribution associated with the involved resonances. We verified that it was not correlated to the discretization mesh used for the calculation.

At the main resonance we then obtain a rather homogeneous field distribution in the gap, the amplitude reaching almost 100 times that of the illumination amplitude [$\lambda = 404\,\mathrm{nm}$, Fig. 6(a)]. For larger separation distances d, the field enhancement at the main resonance is much smaller than for $d = 2\,\mathrm{nm}$, as already observed in Fig. 4. The amplitude in the gap reaches now about 18 for $d = 10\,\mathrm{nm}$ [Fig. 6(b)], and about 12 for $d = 20\,\mathrm{nm}$ [Fig. 6(c)]. Contrary to the $d = 2\,\mathrm{nm}$ case, no higher modes can now be resolved for these separation distances.

The SCS for intersecting cylinders ($d = -2, -5$, and $-20\,\mathrm{nm}$) is shown in Fig. 7. For $d = -2\,\mathrm{nm}$ we observe a very complex spectrum: Several resonances are excited, spanning a large wavelength range between 340 nm and 583 nm. When the cylinders intersect further ($d = -5\,\mathrm{nm}$ and $d = -20\,\mathrm{nm}$), the spectra become less complex, and the resonances are blue–shifted. The reason for this is rather obvious: For larger intersection the spectrum will finally converge to that of a single cylinder.

The "main resonance" reported in Fig. 3 for $d < 0$ was not the first but the second resonance, from the right in Fig. 7. Indeed, this resonance can be seen as the continuation

#33954 - $15.00 US
Received May 09, 2001; Revised May 25, 2001

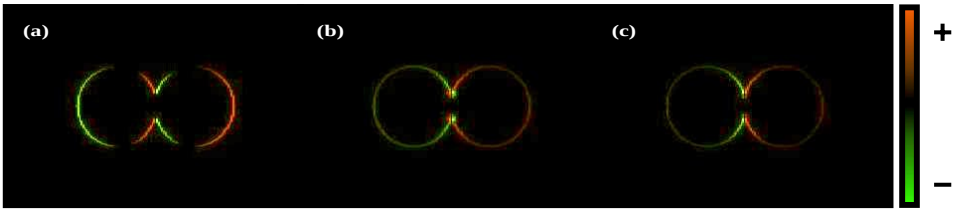

Fig. 8. Polarization charge distribution for two intersecting 50 nm cylinders (d = −2 nm) for the resonances at (a) $\lambda = 338$ nm, (b) $\lambda = 430$ nm, (c) $\lambda = 540$ nm.

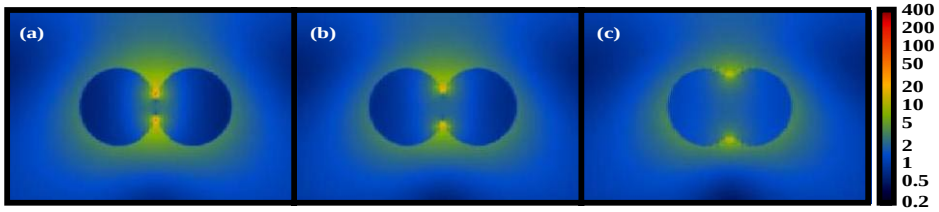

Fig. 9. Field amplitude distribution as a function of the illumination wavelength (indicated on the top of each frame) for two intersecting cylinders illuminated from the top. Different intersection distances are investigated: (a) d = −2 nm (634 KB), (b) d = −5 nm (511 KB), and (c) d = −20 nm (386 KB). Front pictures: Corresponding main resonances (a) $\lambda = 430$ (nm), (b)$\lambda = 404$ (nm), (c) $\lambda = 384$ (nm).

of the main resonance for two interacting (but non–touching) cylinders, as illustrated in Fig. 8. In that figure we report the polarization charge distribution associated with three resonances of the $d = -2$ nm intersecting cylinders. As charges can now flow over both cylinders, the fundamental mode has minus charges on one cylinder and plus charges on the other one [$\lambda = 540$ nm, Fig. 8(c)]. The next resonance, $\lambda = 430$ nm, Fig. 8(b), has charges of both species on each cylinder, as was the case for non–touching cylinders [compare with Fig. 3(b)]. It is associated with strongly confined charges of opposite signs around each grooves. These first two resonances provide the strongest near–field enhancement. The next order modes for intersecting particles have a fairly complex charges distributions, with rapid changes of signs over small distances. The last charges distribution reported in Fig. 8 corresponds to a resonance very similar to that of individual cylinders [$\lambda = 338$ nm, Fig. 8(a)]. Contrary to the two previous resonances, where the charges were mainly concentrated around the grooves, a fairly homogeneous charges distribution on the entire surface of each cylinder is observed at $\lambda = 338$ nm [Fig. 8(a)].

The movies in Fig. 9 show the field distributions corresponding to the SCS reported in Fig. 7. For the small intersection [$d = -2$ nm, Fig. 9(a)], we recognize higher order modes between 348 nm and 384 nm. Since the spectral spacing between these modes is smaller than their width, a complex changing "interference" pattern is observed in the grooves (we verified that these patterns were not related to our discretization grid). The field enhancement in the groove exceeds 100 for the two resonances corresponding to the largest wavelengths ($\lambda = 430$ and 538 nm). This enhancement is concentrated on a very small area.

For d = −5 nm the field distribution is similar, but with a smaller field amplitude. For d = −20 nm the field amplitude is much smaller, as the grooves angle opens and charges are less easily confined

#33954 - $15.00 US
Received May 09, 2001; Revised May 25, 2001

3. Conclusions

We have investigated the influence of the coupling between two metallic nanowires, on their spectrum of plasmon resonances. Our results show that this coupling becomes extremely important for small separation distances, leading to additional resonances in the overall structure. These resonances produce extremely strong electromagnetic fields in the gap between the particles. The topology of these different modes was related to the distribution of polarization charge. A similar enhancement was also observed in the grooves between intersecting particles.

Although not shown here, we observed similar enhancement factors for nanowires with dimensions in the 20–80 nm.

The near–field enhancement observed, with an electric field amplitude excessing hundred times the illumination amplitude, provides an important mechanism for SERS. The magnitude of this enhancement is sufficient for explaining recent SERS experiments where single molecule sensitivity was achieved [19, 20, 21]. Remarkably, this enhancement is obtained in interacting particles with a very simple shape and does not require complex geometries such as fractal system [39].

The rapid variations of the resonances spectrum as a function of the particles configuration that we observed, provides an explanation for the spectral insensitivity of the Raman signal measured on large ensembles of molecules deposited on a colloidal substrate. As a matter of fact, such a substrate contains many different particles with different sizes and spacing, so that coupled plasmon resonances are likely to be excited irrespective of the illumination wavelength.

Acknowledgments

We are most indebted to S. Schultz and D.R. Smith who triggered our interest for plasmon resonant nanoparticles. This work was supported by the Swiss National Science Foundation.

#33954 - $15.00 US Received May 09, 2001; Revised May 25, 2001